r
Biogeosciences Discuss., 11, 9629–9665, 2014
www.biogeosciences-discuss.net/11/9629/2014/
doi:10.5194/bgd-11-9629-2014

Biogeosciences Discussions
Open Access

Evaluating Southern Ocean biological production in two ocean biogeochemical models on daily to seasonal time-scales using satellite surface chlorophyll and O_2/Ar observations

B. F. Jonsson[1], S. Doney[2], J. Dunne[3], and M. L. Bender[1]

[1]Department of Geosciences, Princeton University, Princeton, New Jersey, USA
[2]Marine Chemistry and Geochemistry Department, Woods Hole Oceanographic Institution, Woods Hole, Massachusetts, USA
[3]Geophysical Fluid Dynamics Laboratory, NOAA, Princeton, New Jersey, USA

Received: 3 April 2014 – Accepted: 7 May 2014 – Published: 20 June 2014

Correspondence to: B. F. Jonsson (bjonsson@princeton.edu)

Published by Copernicus Publications on behalf of the European Geosciences Union.

Abstract

We assess the ability of ocean biogeochemical models to represent seasonal structures in biomass and net community production (NCP) in the Southern Ocean. Two models are compared to observations on daily to seasonal time scales in four different sections of the region. We use daily satellite fields of Chlorophyll (Chl) as a proxy for biomass, and in-situ observations of O_2 and Ar supersaturation (ΔO_2Ar) to estimate NCP. ΔO_2Ar is converted to the flux of biologically generated O_2 from sea to air ("O_2 bioflux"). All data are aggregated to a climatological year with a daily resolution. To account for potential regional differences within the Southern Ocean, we conduct separate analyses of sections south of South Africa, around the Drake Passage, south of Australia, and south of New Zealand.

We find that the models simulate the upper range of Chl concentrations well, underestimate spring levels significantly, and show differences in skill between early and late parts of the growing season. While there is a great deal of scatter in the bioflux observations in general, the four sectors each have distinct patterns that the models pick up. Neither model exhibit a significant distinction between the Australian and New Zealand sectors, and between the Drake Passage and African sectors. South of 60° S, the models fail to predict the observed extent of biological O_2 undersaturation. We suggest that this shortcoming may be due either to problems with the ecosystem dynamics or problems with the vertical transport of oxygen.

Overall, the bioflux observations are in general agreement with the seasonal structures in satellite chlorophyll, suggesting that this seasonality represent changes in carbon biomass and not Chl : C ratios. This agreement is shared in the models and allows us to interpret the seasonal structure of satellite chlorophyll as qualitatively reflecting the integral of biological production over time for the purposes of model assessment.

BGD
11, 9629–9665, 2014

1 Introduction

Recent years have seen an intense effort to better understand the global biogeochemical cycle. Scientific cruises organized by programs such as CLIVAR, GLODAP, and GEOTRACES have generated a wealth of data, some of which have been aggregated to climatologies of physical and chemical tracers in the global oceans (e.g. Garcia et al., 2010). Field data and satellite observations of phytoplankton biomass have also helped us to assess the mean state and variability of the global marine ecosystem. Concurrently, a number of ocean global general circulation models (OGCMs) with added functionality to simulate biogeochemical processes have been developed, mainly to study trends and variability in earth's climate and the global carbon cycle.

One specific challenge for OGCMs is to simulate vertical exchange of water and tracers in the ocean. Most physical processes that generate vertical mixing and advection act on length-scales several orders of magnitude smaller than the model resolution. Numerical methods with different types of parameterizations have been developed to mimic the effect of such small-scale dynamics (e.g., boundary layer dynamics, diapycnal mixing, and isopycnal mixing). Global climate models are normally tuned to simulate large-scale processes such as the global wind-driven and thermohaline circulation, hydrography and water mass distributions (e.g. temperature, salinity fields), and are optimized to have a high skill in simulating the exchange of water and tracers between the surface ocean and deeper waters below the thermocline (Large et al., 1997; Doney et al., 2007). Their skill is evaluated by comparing model simulations with observed global distributions of transient tracers (e.g., radiocarbon and chlorofluorocarbons), especially in the deep sea. The boundary layer parameterizations embedded in OGCMs are also often tested in 1-D against high-frequency observations (e.g. Large et al., 1994).

This approach is appropriate for evaluations of model skill on annual to decadal timescales but does not assess how well models simulate underlying processes that act on daily to seasonal scales. An increased interest in bio-physical interactions on

BGD
11, 9629–9665, 2014

smaller temporal and spatial scales, together with the recent ability to run global eddy-resolving OGCMs have also contributed to the need for determining the skills of 1° resolution OGCMs on these timescales. It is, for example, possible that a model with high skill in estimating annual mean phytoplankton biomass does not correctly simulate process-level details in the seasonal cycle of biological production.

Recent studies suggest that high-resolution eddy resolving models have significantly stronger vertical mixing than coarser models. Sallee and Rintoul (2011) found, for example, that subduction rates were up to 4 times higher in the 1/6° ECCO model of the Southern Ocean than in a model with 1° resolution. Their results also show large variations in vertical mixing and subduction between different areas of the model domain. Another example is a study by Karleskind et al. (2011) where the investigators modeled the physics and biogeochemistry for a 750 km × 500 km box in the eastern North Atlantic with a 1 km resolution model. Their results suggest that subduction is more important than air–sea exchange for removing oxygen from the mixed layer over annual time-scales in this region. Such findings would indicate that the vertical transport of O_2 is larger than normally seen in GCMs with lower resolution.

While these studies both raise important questions about how the models' spatial resolution might affect vertical mixing and advection, they are still model-to-model comparisons. In the analysis, it is also important to include observations in the analysis that reflect the exchange between the mixed layer and the mesopelagic zone on daily to monthly timescales. The observed property must be dynamic in the sense that it has natural sources and sinks large enough to significantly change the concentration on the order of days to week. It is also beneficial if sources and sinks are vertically separated from each other.

One promising candidate with such characteristics is the ratio of supersaturation between oxygen and argon (ΔO_2Ar). This quantity is influenced by both biological processes on short timescales and vertical transport across the base of the mixed layer, and can hence be used to give a combined evaluation of how well models simulate upper ocean biogeochemical rate processes, sea–air O_2 fluxes, and vertical mixing.

BGD
11, 9629–9665, 2014

Such an integrated assessment is valuable since the interaction between physics and biology is a key source for variability on short timescales (days to months). A possible further conversion is to combine ΔO_2Ar with wind data to calculate a flux of biologically generated O_2 from sea to air ("O_2 bioflux"). O_2 bioflux is advantageous because the property is the result of net community production (NCP) in the mixed layer and will be significantly diminished by vertical transport of O_2-undersaturated waters into the summertime mixed layer. The following equation expresses the O_2 balance of the mixed layer (Ducklow and Doney, 2013):

$$dO_2/dt = GPP - R + (-FO_2 + D_{in})/h_{ml} \quad (1)$$

where dO_2/dt is the time rate of change of dissolved oxygen (units of mol m^{-3} day^{-1}), GPP is volumetric gross primary production (same units), R is volumetric community respiration rate (autotrophic and heterotrophic), FO_2 is the sea to air gas exchange flux, D_{in} is net input (or loss) of O_2 to the mixed layer from ocean physics (i.e., mixing and advection), and h_{ml} is the mixed layer depth. Net community production equals production minus respiration: NCP = GPP – R. The oxygen budget of the ocean mixed layer is strongly influenced by exchange with the atmosphere across the air–sea interface.

The ΔO_2Ar method was developed to estimate oceanic net community production (NCP) by measuring the saturation of O_2 and Ar in the mixed layer (e.g. Spitzer and Jenkins, 1989). O_2 supersaturation occurs from both biological O_2 production and physical processes such as warming, changes in air pressure, and bubble entrainment. It is possible to decouple the biological component from the physical component by using the saturation of Ar, since Ar has similar physical properties as O_2 but is biologically inert. Following Craig and Hayward (1987), we define O_2 supersaturation relative to Ar as:

$$\Delta O_2Ar = \frac{(O_2/Ar)_{sample}}{(O_2/Ar)_{eq}} - 1 \quad (2)$$

BGD
11, 9629–9665, 2014

This term is equivalent to the biological O_2 supersaturation. Knowing ΔO_2Ar, one can approximate the loss of biological O_2 via gas transfer across the air–sea interface (hereafter denoted O_2 bioflux) via the relationship

$$O_2\text{bioflux} \approx \kappa \cdot \Delta O_2/Ar \cdot O_2\text{eq} \quad (3)$$

where κ is gas transfer velocity based on Wanninkhof (1992) and O_2eq the concentration of O_2 at equilibrium.

In deriving Eq. (3), we have excluded other processes that influence biological O_2 supersaturation in the mixed layer, especially vertical mixing. In high latitudes and during winter, this process generally causes biological O_2 saturation to decrease, because O_2 is most often undersaturated in waters below the base of the mixed layer during these conditions, whereas Ar is close to saturation. The opposite can be true during the summer for shallow mixed layers, particularly in the subtropics, where a substantial component of NCP (and thus net community O_2 production) occurs below the mixed layer, and there is an O_2 maximum in the shallow seasonal thermocline (Najjar and Keeling, 1997). The O_2/Ar supersaturation is hence influenced by the vertical flux of O_2 between the mixed layer and deeper waters. ΔO_2Ar is insensitive to the noise in O_2 saturation on short timescales from synoptic or seasonal physical processes, such as changes in atmospheric pressure, warming/cooling, and bubble entrainment.

The mixed layer O_2 supersaturation thus reflects the O_2 mass balance between net community O_2 production, losses by O_2 bioflux, downward transport of O_2 from the mixed layer to deeper waters, and upward transport of waters with low oxygen concentrations. One consequence of this balance is a negative relationship between O_2 bioflux and the net downward vertical transport of O_2, at steady-state:

$$\text{NCP} = O_2\text{bioflux} + O_2\text{vertical flux}. \quad (4)$$

Most studies of mixed layer ΔO_2Ar aim to constrain NCP from O_2 bioflux estimates. In some studies, the O_2 vertical fluxes were estimated and Eq. (4) was used to calculate NCP. In other studies, the vertical flux of biological O_2 was assumed to be negligible when calculating NCP (e.g. Reuer et al., 2007; Cassar et al., 2011). The resulting

BGD
11, 9629–9665, 2014

bias in NCP has been diagnosed using models where both NCP and O_2 bioflux are prescribed (Jonsson et al., 2013). Jonsson et al. (2013) found that the influence of biology and physics on O_2 bioflux differed between two ocean models, reflecting choices in physical and biological parameterizations as well as surface forcing and, to some degree, model resolution. Here we compare the spatial and temporal patterns of O_2 bioflux in the same two models with the distribution observed in the Southern Ocean, with the hope that the use of multiple models will highlight both commonalities and model-specific skill and errors.

Our focus in this study is the Southern Ocean south of 40° S. This is a region of critical importance for the global biogeochemical cycle and for the uptake of anthropogenic carbon-two processes connected to the vertical exchange of water between the shallow and deep parts of the ocean. The Southern Ocean is also a key region for the global thermohaline circulation since here deep water is upwelled to the surface, transformed by biological activity and air–sea exchange, and eventually exported as intermediate, mode, or bottom waters. Another benefit with focusing on this region is that a large number of ΔO_2Ar measurements have been collected from this area. In this study, we use measurements from several cruises between 1999 and 2011 that have been reported in Huang et al. (2012); Reuer et al. (2007); Cassar et al. (2011). We compare this dataset with two state-of-the-art global ocean general circulation models which both have the added functionality to simulate O_2 bioflux (Jonsson et al., 2013). The two models have coarse, non-eddy resolving spatial resolutions (1–3°) and are forced by CORE2 synoptically-varying, re-analyzed winds and atmospheric properties.

In this paper, we explore the difference between ΔO_2Ar and O_2 bioflux, compare our observations with model output, and finally discuss what the results tell us about net community production and the summertime exchange between the mixed layer and the mesopelagic.

BGD
11, 9629–9665, 2014

2 Methods

This evaluation is based on combining data from observations, models, and remote sensing. The data from each source have different temporal and spatial resolution and different ranges in time. To compensate for these discrepancies, we re-grid in-situ observations and satellite fields to a model grid with roughly 1° resolution at equal intervals in time We also combine observations from different years but the same year day (e.g. 1 January 2003, 1 January 2004, 1 January 2005) to a climatological year with a daily time resolution.

2.1 Satellite data

We use remotely observed chlorophyll concentrations from MODIS/Aqua on the Level-3 9 km × 9 km grid. Daily satellite images from 2003 to 2010 were aggregated to the model grids and averaged to a year-day climatology. Satellite data, particularly in the Southern Ocean, suffers from a high frequency of days where clouds, light conditions, sea-ice, or other problems disqualify the observations. The relative frequency of such days for our dataset is between 5 % and 15 % on the original grid and between 20 % and 50 % on the aggregated model grid.

2.2 In-situ observations

We use ΔO_2Ar observations from 19 Southern Ocean cruises between 1999 and 2009, all occurring during the austral summer. The geographical locations of the respective ship tracks are presented in Fig. 2. The measurements were conducted by two different methods: water was collected in bottles and analyzed in lab (shown as blue in Fig. 2) on 16 cruises, and ΔO_2Ar was measured directly using a ship-borne flow-through system in 3 cruises (shown as red in Fig. 2). The measurements are clustered in space and time reflecting tracks of the ships of opportunity used in this study. We use these sampling clusters in our analysis as natural areas to compare and contrast different parts

BGD
11, 9629–9665, 2014

of the Southern Ocean. A more detailed description of the sampling strategies and measurement methods can be found in Reuer et al. (2007) and Cassar et al. (2009, 2011).

Bioflux is calculated as the product of the biological O_2 supersaturation and the gas transfer velocity. The latter is determined using the Wanninkhof (1992) parameterization expressing gas transfer velocity in terms of a quadratic function of wind speed and the Schmidt number. We do the calculation using daily averages of the NESDIS wind product with a 0.5° resolution based on data from the QuikSCAT satellite (Ebuchi et al., 2002). The gas transfer velocity for each ΔO_2Ar measurement is calculated from the daily-mean local wind speeds during the 60 days preceding collection. A time-weighted value for the gas transfer velocity is calculated based on the fraction of the mixed layer flushed in each subsequent interval until sampling (Reuer et al., 2007; Bender et al., 2011). The resulting gas transfer velocity is then used in Eq. (3) to calculate O_2 bioflux from ΔO_2Ar supersaturation. A detailed analysis of possible uncertainties affiliated with the method can be found in Jonsson et al. (2013).

2.3 Models

The observations are compared with output from the ocean components of two IPCC-class ocean biogeochemical models. The TOPAZ ocean model is built upon version 4 of the modular ocean model (MOM4 Griffies et al., 2005) with a vertical z-coordinate and a horizontal B-grid with a tri-polar coordinate system (North America, Siberia, and Antarctica) to resolve the Arctic. The model has a nominally 1-degree horizontal resolution globally with higher meridional resolution near the equator (to 1/3°). There are 50 vertical layers; resolution is 10 m in the upper 200 m, and coarser below. MOM4 includes a representation of the k-profile parameterization (KPP) planetary boundary layer scheme (Large et al., 1994), Bryan–Lewis deeper vertical mixing, Gent–McWilliams isopycnal thickness diffusion (Gent and McWilliams, 1990), bottom topography represented with partial cells, isotropic and anisotropic friction, and a multiple dimensional flux limiting tracer advection scheme using the third order Sweby flux

BGD
11, 9629–9665, 2014

limiter. For these studies, the ocean model is forced by prescribed boundary conditions from the reanalysis effort of the ECMWF and NCAR Common Ocean-ice Reference Experiments (CORE).

BGCCSM is based on the Los Alamos National Laboratory Parallel Ocean Program (POP) (Smith and Gent, 2004). In our application, the grid is symmetric in the Southern Hemisphere with a zonal resolution of 3.6°. Meridional resolution decreases from 1.8° at mid-latitudes to about 0.8° at high and low latitudes. The surface layer is 12 m thick; there are in total 5 layers to 111 m, and 25 layers to the bottom. This model invokes Gent–McWilliams' isopycnal mixing and the KPP upper ocean model, and is also forced by prescribed boundary conditions from CORE.

The air–sea fluxes of O_2 and CO_2 in both models are computed using prescribed atmospheric conditions (surface pressure, mole fraction), model-predicted surface water concentrations, NCEP surface winds, and the quadratic dependence of the gas exchange coefficient on wind-speed model of (Wanninkhof, 1992). Argon was added as a prognostic tracer to the simulations in both models in an analogous fashion to O_2; i.e., O_2 and Ar solubility are similarly determined using model temperature and salinity, and Ar uses the same gas-exchange parameterization as O_2.

Both models include complex biogeochemistry/ecosystem components with macro- and micronutrients, organic matter, and three phytoplankton functional groups: small phytoplankton, large phytoplankton, and diazotrophs. Both invoke co-limitation by iron, light, and nitrogen, mediated in part by their influence on the Chl : C ratio, and slower rates of photosynthesis at lower temperatures. Diazotrophs have high N : P ratios and low photosynthetic efficiencies (TOPAZ) or high iron requirements (TOPAZ, BGCCSM). It is possible to use either ΔO_2Ar or O_2 bioflux for comparing observations with models. One could argue that ΔO_2Ar is a more robust property since it is an observed quantity, whereas O_2 bioflux is a derived product that depends on the wind field. On the other hand, model ΔO_2Ar depends on the choice of wind forcing, whereas O_2 bioflux is assumed to be mainly controlled by NCP. Our tests show that both methods give similar

BGD
11, 9629–9665, 2014

accuracy and we choose to use O_2 bioflux since its units are more appropriate for the current study (see Sect. 5 for further discussion).

3 Results

First we test the feasibility of aggregating data from different years into a single climatological year. This approach is useful only if the difference between seasons is significantly larger than the inter-annual variability. We test the assumption by comparing how model O_2 bioflux changes from one date to another in a climatological year, against the standard deviation at the same dates between a number of years. Fields from BGCCSM were used to generate climatologies for the days 15 November and 15 December by averaging data for the entire Southern Ocean from four consecutive model-years. Our results show that the mean difference is 19.8 mmol O_2 m^2 d^{-1} between the two different dates, whereas the standard deviation over four years on the respective dates is only 8.7 mmol O_2 m^{-2} d^{-1}. It is hardly an unexpected result that spring values of O_2 bioflux differs from summer since the Southern Ocean is a high-latitude region. This result encourages us to aggregate observations and model-data from different years into a climatological year.

Next, we compare the model simulations with observations. Chlorophyll simulated by BGCCSM and TOPAZ is related to satellite observations retrieved by the MODIS/Aqua mission from 1 January 2003 to 31 December 2010. Each daily satellite image is reprojected from a native 9 km × 9 km resolution to the TOPAZ' 1° × 1° grid and the fields are aggregated to a climatological year, as mentioned earlier. The resulting datasets are analyzed in four geographical sectors, shown as shaded areas in Fig. 2. We zonally average the data in each sector to a Hofmøller diagram with latitude on the y-axis, time on the x-axis, and daily zonal Chl averages as colors (Figs. 3–6). It should be noted that one problem with using satellite-retrieved Chlorophyll is a systematic lack of data during winter due to low light conditions and sea-ice cover in combination with the satellite's track. These periods are shown as gray areas in the figures.

BGD
11, 9629–9665, 2014

Figures 7–10 present model NCP and bioflux vs. our observations. Panel a in each figure shows the temporal evolution of NCP vs. latitude in the two models, and panel b the corresponding model O_2 bioflux. The sampling locations are indicated on the model plots by gray circles. Panel c, finally, presents O_2 bioflux from the observations shown in Fig. 2. As mentioned earlier, all measurements that fall on the same year-day and grid cell are combined to one mean value, which is indicated by the color of the dot. Note that the aggregated values of observed O_2 bioflux presented together with TOPAZ are somewhat different from the ones connected to BGCCSM, since the two model grids are different.

A general pattern arises where the models simulate upper ranges of Chl well but underestimate spring levels significantly. Both models also show differences in skill between early and late parts of the growing season, performing better during the spring and early summer. While there is a great deal of scatter in the bioflux observations, the four sectors each show distinct patterns, wheras the models exhibit little distinction between the Australian and New Zealand sectors, and between the Drake Passage and African sectors. Next, we compare the simulated fields and data for each of the study regions in more detail.

3.1 Drake passage

The seasonal change in satellite-derived Chlorophyll for the Drake Passage sector is shown in Fig. 3a. It is possible to discern a seasonal cycle, even if we lack winter and early spring data in higher latitudes. Towards to South, the earliest retrieved concentrations are between 3 and 5 times lower than maximum values at late spring/summer peak. Both the magnitude and timing of maximum summer Chl concentrations vary with latitude, with the strongest and latest blooms occurring in high latitudes. [Chl] reaches $1\,\mathrm{mg\,m^{-3}}$ south of 70° S, decreases to $0.5\,\mathrm{mg\,Chl\,m^{-3}}$ between 60° S and 70° S, and increases again north of 50° S. The growing season, as inferred from the period of elevated summer Chl, is about three months south of 70° S and generally lengthens

BGD
11, 9629–9665, 2014

going to the north. The band of very high Chl north of 45° S is likely due to transport of sedimentary iron from coastal waters generating elevated biological production.

Panels b and c present Chl climatologies from TOPAZ and BGCCSM. The grey shadings indicate where satellite coverage is missing. It is clear that the seasonal chlorophyll progression in both models diverge from observations, whereas the magnitude of peak Chl concentrations is simulated rather well. TOPAZ underestimates Chl concentrations somewhat early in the season and generates an intense spring bloom extending over the entire sector from 75° S to 40° S. ("Bloom" as used here indicates a transient period of high [Chl] lasting no more than 1 month.) In the observations high [Chl], once established, continues throughout most of the summer, and concentrations $> 1\,\mathrm{mg\,m^{-3}}$ are limited to the region south of 70° S. In these southern regions, the onset of the TOPAZ bloom comes 1–2 months earlier than in the observations. The spring bloom in TOPAZ collapses after about a month with too low concentrations of Chl over the austral summer as a result. Finally, the season ends with TOPAZ generating a weaker fall bloom during part of the season without satellite coverage. South of 50° S, BGCCSM begins the season with much lower Chl concentrations than both TOPAZ and satellite observations. The model generates a much more intense bloom between 60° S and 70° S than observations suggest, but has good skill in predicting the timing and magnitudes south of 70° S. Both models suggest that during the bloom, biomass is significantly higher in the frontal regions compared to observations.

O_2 bioflux observations in the Drake Passage region originates both from transects crossing the Drake Passage and nearby cruises in the Palmer Long Term Ecological Research program annual survey west of the Antarctic Peninsula. Our results are thus partly influenced by coastal processes outside the models' domain. In the Drake Passage sector, TOPAZ and BGCCSM show similar patterns in NCP (panel a) north of 65° S. South of 65° S, TOPAZ simulates intensive NCP over the summer, whereas BGCCSM has close to zero net production. Both models have predominantly negative O_2 biofluxes south of 50° S in October (panel b), and a progressive change to positive fluxes from north to south with time. The negative values of O_2 bioflux in TOPAZ are

BGD
11, 9629–9665, 2014

about twice as large as they are in BGCCSM. In TOPAZ, O_2 bioflux is positive throughout the domain in January, whereas in BGCCSM there is a southerly region of negative flux throughout the season.

Panel c of Fig. 7 shows observations of O_2 bioflux in the region. The pattern of negative fluxes south of 60° S in November and December corresponds qualitatively with the models. There is a wealth of observations south of 60° S in January and February, but they show significant variability. Some observations suggest biological production rates of up to 50 mmol m^{-2} d^{-1}, which is similar to the levels predicted by TOPAZ. Others correspond to the results from BGCCSM with O_2 bioflux estimates near or below zero. The mean observed O_2 bioflux values in January and February south of 65° S are 8 ± 20 mmol O_2 m^{-2} d^{-1}. The corresponding values for BGCSSM are 9 ± 13, and for TOPAZ, 16 ± 27. The observations in April suggest undersaturated conditions that correspond with BGCCSM but not with TOPAZ.

3.2 South Africa

The observations in the South Africa sector (Fig. 4a) show similar patterns to the Drake Passage sector for satellite-derived Chl, with the main exception of a weaker bloom north of 50° S. Note the lack of observations south of 70° S where of Chl concentrations may be very high. TOPAZ (panel b) begins the season with somewhat higher concentrations of Chl than observed and, with time, generates a significantly stronger bloom. As in the Drake Passage, the TOPAZ bloom crashes mid-summer, after which model Chl concentrations are significantly lower than observations. BGCCSM starts the season with much lower Chl concentrations than the satellite data and generates an exaggerated bloom as well, especially south of 55° S.

NCP and O_2 bioflux climatologies (Fig. 8) show that TOPAZ has an earlier and more intense band of positive NCP than BGCCSM (panel a). BGCSSM has a slow southward progression of the the positive NCP band with NCP reaching 20 mmol m^{-2} d^{-1} at 40° S in October and at 65° S in February. TOPAZ, on the other hand, has a more uniform pattern in which most of the region reaches these levels of NCP by mid-November. The two

BGD
11, 9629–9665, 2014

models have O_2 bioflux patterns (shown in panel b) that vary in a fashion similar to that of the Drake Passage region. Both models start with negative O_2 bioflux: $< -30\,m^2\,d^{-1}$ in TOPAZ and $\sim -10\,mmol\,m^{-2}\,d^{-1}$ in much of the domain in BGCCSM. This negative bioflux switches to positive values faster in TOPAZ than in BGCCSM, most likely due to the earlier onset of biological production. Finally, BGCCSM has a slightly earlier and stronger switch to negative O_2 bioflux at the end of the growing season than does TOPAZ.

We have O_2 bioflux observations from four crossings in the South Africa sector (Fig. 8c) distributed in time from December to late March. The November-December transect has a pattern of weakly positive O_2 bioflux in the north that turns negative below 50° S. Both models show a somewhat different pattern with positive O_2 bioflux south of 50° S as well. While both models show positive values, the observed January transect has predominantly negative biofluxes. Finally, the two transects in March show a pattern with high positive O_2 bioflux in the north and significant negative bioflux at 55° S. BGCCSM has a better skill in recreating these patterns than does TOPAZ.

3.3 Australia and New Zealand regions

The Australian and New Zealand sectors (Figs. 5 and 6) follow the general pattern of Drake Passage and South Africa. The main exception is BGCCSM generating spring blooms further north and in a spottier pattern than in the sectors discussed earlier. In this model, the New Zealand sector has four distinct areas/periods of high Chl concentrations: in January-February south of 70° S, November-December between 60° S and 70° S, January between 45° S and 55° S, and October-November north of 45° S. This peculiar pattern could be due to interactions with hydrology in the frontal regions. The Australian sector show similar patterns for the latter three areas whereas the region south of 70° S lack data. TOPAZ shows indications of being out of phase with both MODIS and BGCCSM, whereas BGCCSM captures the seasonal cycle in MODIS better.

BGD
11, 9629–9665, 2014

NCP climatologies from the Australian sector (Fig. 9a) show that TOPAZ generates short intense periods of positive NCP early in the growing season. In the southern reach of the domain, NCP stays high into the fall whereas elsewhere summer and fall NCP values are low (10 mmol m^{-2} d^{-1}). BGCCSM, on the other hand, has a much longer and more intense period of positive NCP than in other parts of the Southern Ocean. In this model, spring conditions south of 45–50° S are dominated by weaker negative O_2 biofluxes when compared to other regions in both models (panel b). BGCCSM switches to negative bioflux at the end of the summer whereas O_2 bioflux in TOPAZ stays positive throughout March.

The observations in this part of the ocean differ from those simulated by TOPAZ. For example, almost all measurements north of 55° S report higher O_2 biofluxes, > 25 m^2 d^{-1}, in February. As well these field data exhibit low or even negative biofluxes at 65° S where TOPAZ predicts strong biological production and high O_2 bioflux from mid-November to mid-February. BGCCSM is more in line with observed patterns, with the main exception of an early onset of negative O_2 bioflux in the fall at 40° S–50° S in the model where the observations still suggest strong positive biofluxes. In general, between 50 and 60° S, TOPAZ and BGCCSM both simulates a strong spring bloom whereas observations show a simpler patters of sustained high production throughout the latter part of spring and summer. Model NCP and O_2 bioflux in the New Zealand region are similar to values in the Australian sector (Fig. 10a and b). The O_2 bioflux observations in panel C show considerable scatter but in general are marked by high values north of the Polar front at 60° S, with low or negative values of bioflux to the south at most times. Both models capture the highly negative values of bioflux early in the growing season south of 60–65° S, and occasionally negative values of bioflux later in the growing season. BGCCSM simulates our observations of sustained high NCP north of the Polar Front from November through February.

BGD
11, 9629–9665, 2014

3.4 Cross regional, Southern Ocean analysis

The data-model comparisons of O_2 bioflux for the different regions have certain patterns in common. In both models, the spring period of strong positive flux starts later in high latitudes. In general, TOPAZ tends to have an earlier, shorter, and more intense period of high Chl concentrations, than does BGCCSM. Observed values of O_2 bioflux are much more variable than simulated values. This is expected given the relatively smooth and coarse fields of the models, and likely reflects the absence of mesoscale processes in the models.

Our next step is to compare the seasonal range in O_2 bioflux values between observations and models as a function of latitude (Fig. 11). We aggregate the observations to year-days and model grid-cells as described above, but compare the resulting values with corresponding individual data points in the models matched by both location and collection time. Such comparison using individual data points suffers more from small-scale spatial mismatches than the zonal model averages used earlier, but allows us to better compare the seasonal range of O_2 bioflux values between models and observations. Figure 11 shows O_2 bioflux vs. latitude for the two models and observations in each of the previously defined regions. We find that BGCCSM generally predicts the meridional variability of ranges in O_2 bioflux, suggesting that processes constraining NCP are simulated well. The seasonal maximum of model O_2 bioflux might not occur at the same time in the models as in the real world, but the magnitude of the maximum values seems to be fairly well predicted. Equator-ward of about 60° S the models also tend to capture the fact that bioflux is seldom < 0, reflecting both low wintertime NCP and physical transport. In contrast, the models do not capture well the observed strong negative O_2 bioflux at high latitudes. TOPAZ also tends to exaggerate high positive O_2 bioflux in some areas, such as 60° S–70° S in the Drake Passage and New Zealand regions, whereas O_2 bioflux is underestimated in TOPAZ between 40° S and 50° S in the Australian and New Zealand regions.

BGD
11, 9629–9665, 2014

Finally, we compare observed and simulated O_2 bioflux values for the same locations and times. The scatter plot in Fig. 12 compares O_2 bioflux simulated by TOPAZ (blue) and BGCSSM (red) with observations binned to the same year-days on the respective model's grid. It is clear from this figure that both models show a low correlation with the observations ($r^2 = 0.024$ for TOPAZ and $r^2 = 0.23$ for BGCCSM). This low correlation is expected: lags in time or displacements in space can generate large differences between the models and observations even if the fundamental processes are simulated with high skill (Doney et al., 2009). Further, the field data contain mesoscale variability that cannot be captured in the models (even if the models were eddy-resolving, the details of the simulated turbulent fields would differ from observed). It is also clear that the distributions of model-data residuals (difference from a diagonal 1 : 1 line) are asymmetrical. The upper right quadrant, where both observations (obs) and model data (mod) are positive, has considerable scatter about the 1 : 1 line but no apparent bias. The lower right quadrant (negative model, positive observation) is mainly empty, showing that the model rarely predicts undersaturation when the observations report supersaturation. An exception is the clustering of TOPAZ NCP values about zero, a consequence of low production simulated by that model after an intense bloom. The upper left quadrant is heavily populated, showing that the models frequently simulate positive values of bioflux when the ocean is in fact undersaturated. Consistent with this pattern, the results in the lower left quadrant show that, when data and models agree that bioflux is negative, the observations are more negative than the models. The overall picture is that both models have a positive bias in predicting bioflux, mainly due to fewer negative values compared to the observations (Fig. 12). For all data points the model bias is statistically significant for both a paired t test (BGCCSM: $n = 271$, $t = -4.803$, $p = 0.000$; TOPAZ: $n = 273$, $t = -2.870$, $p = 0.004$) and a one-tailed binomial test (BGCCSM: pos = 167, tot = 271, $p = 0.00005$; TOPAZ: pos = 151, tot = 273, $p = 0.035$). Neither model shows a statistically significant bias when only positive values are considered.

BGD
11, 9629–9665, 2014

4 Discussion

When comparing model and satellite climatologies of Chl concentrations and O_2 bioflux, we find both similarities and significant differences. The models are able to predict spring and summertime maximum levels of Chl and O_2 bioflux well, but generate much too low values of Chl in the onset of the spring season. Such underestimations are particularly important in the case of Chl, which by nature has a lognormal distribution (Campbell, 1995) and is hence skewed towards low values. One explanation for this behavior is a combination of model grazing and/or phytoplankton mortality being too strong in the winter, as reported for the BGCCSM in the sub-polar North Atlantic by Behrenfeld et al. (2013). These patterns could also be explained by the two models simulating too weak vertical export of phytoplankton during summer and too strong export during winter. Johnson et al. (2013) has shown that MODIS/Aqua generally underestimate the dynamical range of Chl in the Southern Ocean, which would suggest that these differences might be even larger.

Another general pattern is that the models tend to simulate the increases in Chl during spring and early summer rather well, but show highly diverging behavior later in the season. In TOPAZ, the ecosystem tends to crash in early January with much too low biomass as an effect, whereas BGCCSM has patches where far too much Chl is produced. This difference between early and late parts of the summer season can be explained by which processes control the ecosystem behavior at different times. The spring bloom onset is thought to be controlled mainly by physical factors such as light, temperature, and vertical stratification, and the summer peak magnitude is controlled by nutrient availability, grazing, mortality, and other ecological and biogeochemical factors (Hashioka et al., 2014). The decrease of Chl concentrations after a summer peak depends mainly on ecosystem dynamics such as grazing, succession, and other interactions between organisms, as well as vertical export of particulate organic matter. Phytoplankton production are in general better resolved by the models, whereas autotrophic processes and vertical transports are challenging to implement well to the

BGD
11, 9629–9665, 2014

models. There processes are often stochastic in their behavior and there is a lack of observation to parameterize them accurately.

Even if the two models generally predict summer season ranges of O_2 bioflux in the Southern Ocean north of 60° S well, there are large regional variations. The differences tend to follow patterns in Chl concentrations discussed earlier, both when comparing the two models with each other and when comparing the models with observations. We also find different and varying patterns in the seasonal cycle of biological net community production, with TOPAZ often having a shorter, more intense growing season than BGCCSM.

One important difference between models and observations is that models fail to predict observed events of negative O_2 bioflux in waters south of 60° S. We suggest two possible explanations for why the models lack these events: problems with the ecosystem dynamics and problems with the vertical transport of oxygen. It is possible that observed summertime undersaturation is generated by net heterotrophy (negative NCP) temporally decoupled from earlier biological production. O_2 supersaturation from periods of positive NCP would then be lost via air–sea exchange before the start of net-respiration. It is also necessary for particulate organic carbon to remain long enough in the mixed layer to be respired, and hence particle export has to be limited. Such events have been observed during the GasEx III experiment (Hamme et al., 2012) but are not generated by either model. Both TOPAZ and BGCCSM simulate NCP to evolve more smoothly than observations across time and space, even if significant variability is seen (Jonsson et al., 2013).

Our second explanation to why models fail in capturing summertime mixed layer O_2 undersaturation is that they underestimate rates and characteristics of vertical mixing. Several studies have shown the potential for entrainment and submeso-scale processes to transport waters between the thermocline and the mixed layer on short time scales. Such events would introduce O_2 undersaturated waters into the mixed lay and generate the type of conditions we find in our observations. OGCMs such as TOPAZ

BGD
11, 9629–9665, 2014

and BGCCSM lack the spatial resolution to resolve these kinds of processes and hence the ability to generate the undersaturated conditions we observe.

We cannot conclusively disprove either explanation for the models' failure to produce negative O_2 bioflux in summer but other studies support the suggestion that vertical transport is an important factor. Simulations by Lachkar et al. (2007); Sallee and Rintoul (2011), both find much stronger subduction rates south of 60° S when comparing high resolution models to ones with lower resolution such as TOPAZ and BGCCSM. The areas of increased subduction described by Sallee and Rintoul correspond very well with the latitude bands where we observe undersaturated conditions not generated by the models. (Below 60° S for the New Zealand, Australia, and Drake Passage sections; Between 60° S and 40° S for the South African section.) Other studies furthermore suggest that such physical processes enabled by higher spatial resolutions tend to be episodic in nature, making them prime candidates to generate the undersaturated O_2 conditions seen in our observations.

One might argue that the lower frequency of negative O_2 bioflux in the models is simply due to model overestimation of NCP. Such a conclusion is not consistent with the models' accurate simulations of the seasonal range of positive O_2 bioflux (c.f. Fig. 11). The models appear to selectively overestimate O_2 bioflux when the observations of O_2 bioflux are negative.

5 Conclusions

Both the TOPAZ and BGCCSM models simulate upper ranges of Chl concentrations well but underestimate spring levels significantly. They also show differences patterns in their skill during early and late parts of the growing season. We find a great deal of scatter overall between simulated O_2 bioflux in the models and observed values when the models are sampled in a analogous fashion to the observations. There are, however, distinct patterns in each sections that both models replicate. and the two models generally predict summer season ranges of O_2 bioflux in the Southern Ocean

BGD
11, 9629–9665, 2014

north of 60° S well. South of 60° S, the models fail to predict the observed extent of biological O_2 undersaturation. We suggest that this shortcoming may be due either to problems with the ecosystem dynamics or problems with the vertical transport of oxygen.

To evaluate ΔO_2Ar or O_2 bioflux for comparing observations with models, we use a box model that calculates the evolution of ΔO_2Ar and O_2 bioflux from prescribed time-series of NCP and wind. The box is a 50 m deep water column with no vertical or horizontal advection or mixing. O_2 air–sea exchange is simulated using O_2 saturation and the Wanninkhof (1992) gas transfer velocity parameterization; the exact setup is described in Jonsson et al. (2013). We conduct three experiments with the box model using a time series of NCP from TOPAZ at 160° W, 61° S (Fig. 1a). In the first experiment, represented by the blue lines in panels b–d, we use CORE-2 atmospheric reanalysis winds with a 2° × 2° resolution from the same position as the NCP observations (panel b). The resulting ΔO_2Ar supersaturation and O_2 bioflux are presented in panels c and d respectively. In the second experiment, which is presented with red lines in panels b–d, we instead use Quickscat satellite-derived wind data with a 0.25° × 0.25° resolution from the same location as the NCP, to simulate the effect of a different wind product. When comparing the two cases, we find that O_2 bioflux is a more robust indicator of the underlying ecological behavior (NRMSD = 5.0 %) than ΔO_2Ar (NRMSD = 10.7 %), which we find more sensitive to short-term differences in the wind forcing applied to the model.

This effect, however, is only true if O_2 bioflux is calculated using the same wind history as that used to generate ΔO_2Ar in the box. In the real world, the forcing is the true wind stress. However, O_2 bioflux is calculated with imperfect wind estimates from satellites or atmospheric reanalysis The observed ΔO_2Ar values are fixed and can not be adjusted to compensate for the errors in the winds used to calculate O_2 bioflux. We test the effect of wind errors by using the reanalysis winds to drive the box model and QuikSCAT winds for the O_2 bioflux calculation. The resulting O_2 bioflux of such an experiment, shown as a green line in panel d, has a similar error (NRMSD = 11.3 %) to

BGD
11, 9629–9665, 2014

that of ΔO_2Ar in panel c. Finally, we compare the relative effect of imperfect wind estimates between ΔO_2Ar and O_2 bioflux. Time series of model NCP and wind from 500 locations in the Southern Ocean is used to force our boxmodel in an analogous fashion to the experiment presented in Fig. 2d. We find that O_2 bioflux shows similar errors to ΔO_2Ar, suggesting that both properties are useful for comparing the models and observations. We choose to use O_2 bioflux since the units of flux are more appropriate for the current study.

Acknowledgements. This work was supported in part by funding from National Aeronautic and Space Administration (NASA NNX08AF12G) and National Science Foundation (NSF OPP-0823101).

References

Bender, M. L., Kinter, S., Cassar, N., and Wanninkhof, R.: Evaluating gas transfer velocity parameterizations using upper ocean radon distributions, J. Geophys. Res.-Oceans, 116, doi:10.1029/2009JC0058, 2011. 9637

Campbell, J. W.: The lognormal distribution as a model for bio-optical variability in the sea, J. Geophys. Res.-Oceans, 100, 13237–13254, 1995. 9647

Cassar, N., Barnett, B. A., Bender, M. L., Kaiser, J., Hamme, R. C., and Tilbrook, B.: Continuous high-frequency dissolved O_2/Ar measurements by equilibrator inlet mass spectrometry, Anal. Chem., 81, 1855–1864, 2009. 9637

Cassar, N., DiFiore, P. J., Barnett, B. A., Bender, M. L., Bowie, A. R., Tilbrook, B., Petrou, K., Westwood, K. J., Wright, S. W., and Lefevre, D.: The influence of iron and light on net community production in the Subantarctic and Polar Frontal Zones, Biogeosciences, 8, 227–237, doi:10.5194/bg-8-227-2011, 2011. 9634, 9635, 9637

Craig, H. C. and Hayward, T.: Oxygen supersaturation in the ocean – biological versus physical contributions, Science, 235, 199–202, 1987. 9633

Doney, S. C., Yeager, S., Danabasoglu, G., Large, W. G., and McWilliams, J. C.: Mechanisms governing interannual variability of upper-ocean temperature in a global ocean hindcast simulation, J. Phys. Oceanogr., 37, 1918–1938, 2007. 9631

BGD
11, 9629–9665, 2014

Doney, S. C., Stow, C. A., Jolliff, J., McGillicuddy, D. J., Allen, J. I., Friedrichs, M. A. M., Rose, K. A., and Wallheadg, P.: Skill assessment for coupled biological/physical models of marine systems, J. Marine Syst., 76, 4–15, 2009. 9646

Ducklow, H. W. and Doney, S. C.: What is the metabolic state of the oligotrophic ocean?, A debate, Annu. Rev. Mar. Sci., 5, 525–533, doi:10.1146/annurev-marine-121211-172331, 2013. 9633

Ebuchi, N., Graber, H. C., and Caruso, M. J.: Evaluation of wind vectors observed by QuikSCAT/SeaWinds using ocean buoy data, J. Atmos. Ocean. Tech., 19, 2049–2062, 2002. 9637

Garcia, H. E., Locarnini, R. A., Boyer, T. P., Antonov, J. I., Baranova, O. K., Zweng, M. M., and Johnson, D. R.: World Ocean Atlas, vol. 3 of Dissolved Oxygen, Apparent Oxygen Utilization, and Oxygen Saturation, US Government Printing Office, Washington, DC, 2009 edn., 2010. 9631

Gent, P. R. and McWilliams, J. C.: Isopycnal mixing in ocean circulation models, J. Phys. Oceanogr., 20, 150–155, 1990. 9637

Griffies, S. M., Gnanadesikan, A., Dixon, K. W., Dunne, J. P., Gerdes, R., Harrison, M. J., Rosati, A., Russell, J. L., Samuels, B. L., Spelman, M. J., Winton, M., and Zhang, R.: Formulation of an ocean model for global climate simulations, Ocean Sci., 1, 45–79, doi:10.5194/os-1-45-2005, 2005. 9637

Huang, K., Ducklow, H. W., Vernet, M., Cassar, N., and Bender, M. L.: Export production and its regulating factors in the West Antarctica Peninsula region of the Southern Ocean, Global Biogeochem. Cy., 26, GB2005, doi:10.1029/2010GB004028, 2012. 9635

Johnson, R., Strutton, P. G., Wright, S. W., McMinn, A., and Meiners, K. M.: Three improved satellite chlorophyll algorithms for the Southern Ocean, J. Geophys. Res.-Oceans, 118, 3694–3703, 2013. 9647

Jonsson, B., Doney, S. C., Dunne, J. P., and Bender, M.: Evaluation of the Southern Ocean O_2/Ar-based NCP estimates in a model framework, J. Geophys. Res.-Biogeo., 118, 385–399, 2013. 9635, 9637, 9650

Karleskind, P., Levy, M., and Memery, L.: Subduction of carbon, nitrogen, and oxygen in the northeast Atlantic, J. Geophys. Res.-Oceans, 116, C02025, doi:10.1029/2010JC006446, 2011. 9632

BGD
11, 9629–9665, 2014

Lachkar, Z., Orr, J. C., Dutay, J.-C., and Delecluse, P.: Effects of mesoscale eddies on global ocean distributions of CFC-11, CO_2, and $\Delta^{14}C$, Ocean Sci., 3, 461–482, doi:10.5194/os-3-461-2007, 2007. 9649

Large, W., Doney, S. C., and McWilliams, J. C.: Oceanic vertical mixing – a review and a model with a nonlocal boundary-layer parameterization, Rev. Geophys., 32, 363–403, 1994. 9631, 9637

Large, W. G., Doney, S. C., Danabasoglu, G., and McWilliams, J. C.: Sensitivity to surface forcing and boundary layer mixing in a global ocean model: annual-mean climatology, J. Phys. Oceanogr., 27, 2418–2447, 1997. 9631

Najjar, R. G. and Keeling, R. F.: Analysis of the mean annual cycle of the dissolved oxygen anomaly in the World Ocean, J. Mar. Res., 55, 117–151, 1997. 9634

Reuer, M. K., Barnett, B. A., Bender, M. L., Falkowski, P. G., and Hendricks, M. B.: New estimates of Southern Ocean biological production rates from O_2/Ar ratios and the triple isotope composition of O_2, Deep-Sea Res. Pt. I, 54, 951–974, 2007. 9634, 9635, 9637

Sallee, J.-B. and Rintoul, S. R.: Parameterization of eddy-induced subduction in the Southern Ocean surface-layer, Ocean Model., 39, 146–153, 2011. 9632, 9649

Smith, R. and Gent, P. R.: Anisotropic Gent–McWilliams parameterization for ocean models, J. Phys. Oceanogr., 34, 2541–2564, 2004. 9638

Spitzer, W. S. and Jenkins, W. J.: Rates of vertical mixing, gas-exchange and new production – estimates from seasonal gas cycles in the upper ocean near Bermuda, J. Mar. Res., 47, 169–196, 1989. 9633

Wanninkhof, R.: Relationship between wind-speed and gas-exchange over the ocean, J. Geophys. Res.-Oceans, 97, 7373–7382, 1992. 9634, 9637, 9638, 9650

BGD
11, 9629–9665, 2014

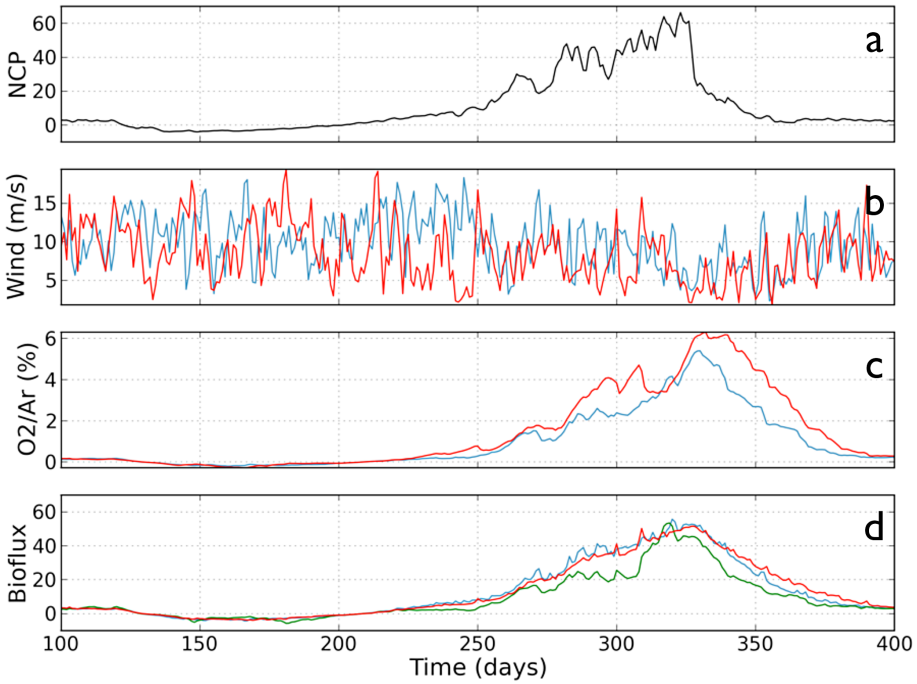

Figure 1. (a) shows mixed-layer integrated NCP from the TOPAZ model at 61.5° S, 159.5° W over a 400 day period. **(b)** shows two wind time-series for the same time. The blue line is the NCEP/CORE reanalysis winds from the same location as the model NCP data, and the red line is Quickscat satellite-derived winds from the same location. The two lines in **(c)** represent the resulting O_2/Ar supersaturation from a box model simulation based on the time series in **(a)** and **(b)**. **(d)** shows O_2 bioflux calculated from the time series in **(b)** and **(c)**. Red line is based on reanalysis winds and ΔO_2Ar, blue line is based on Quickscat winds and ΔO_2Ar, and green line is based on Quickscat winds and ΔO_2Ar calculated from reanalysis winds.

BGD
11, 9629–9665, 2014

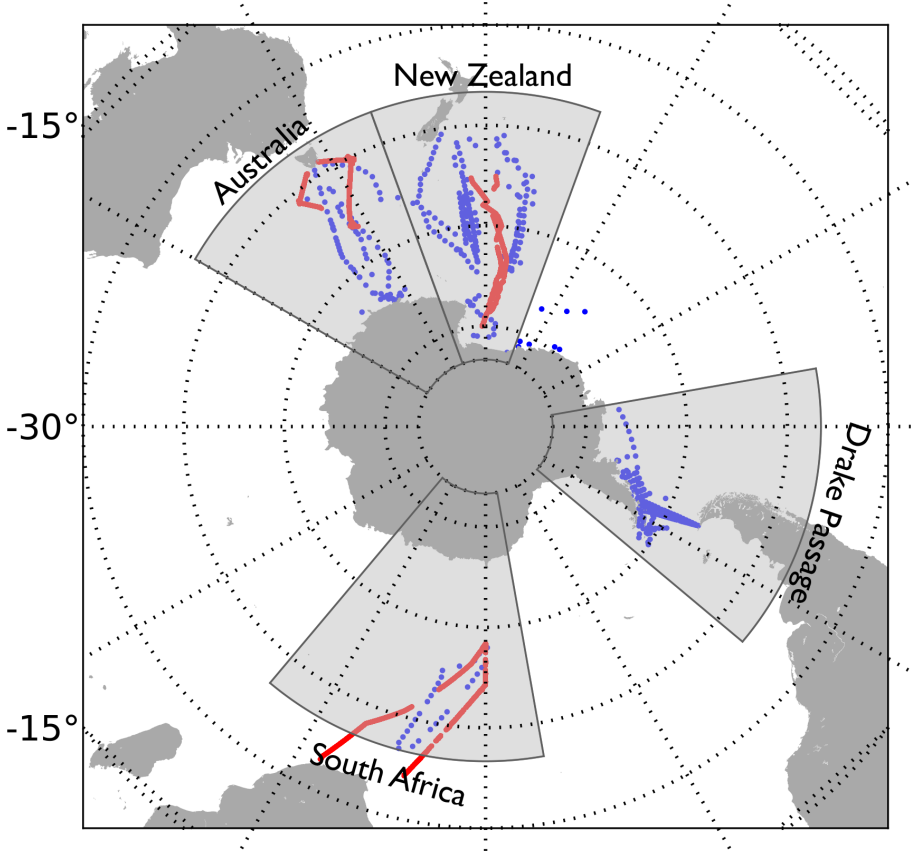

Figure 2. Map of O_2 observations used in the study. Grey shadings signifies the four regions we focus on in this study. Dots indicate discreet sampling locations while red lines indicated continuous sampling.

BGD
11, 9629–9665, 2014

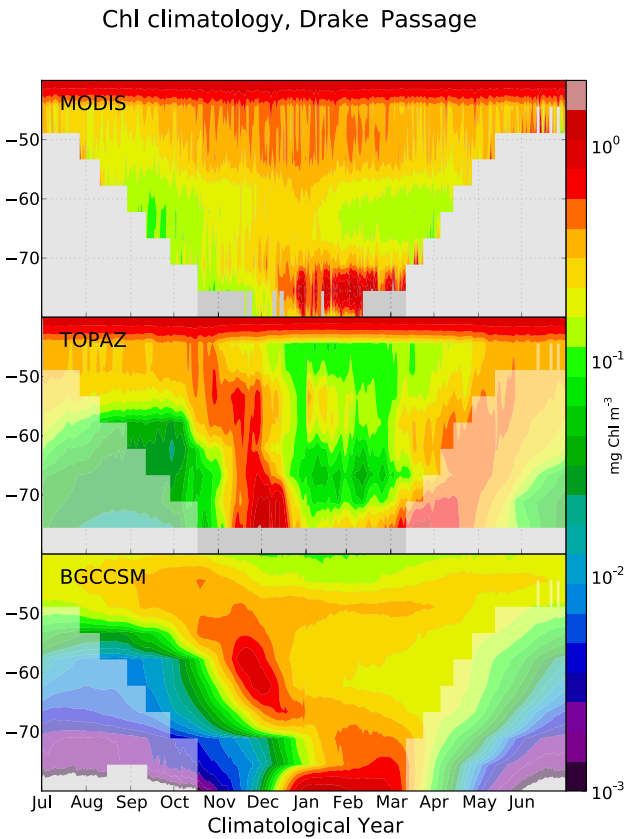

Figure 3. Hofmøller plots of satellite Chl (top panel), Chl simulated by TOPAZ (middle panel), and Chl simulated by BGCCSM (bottom panel) in Drake Passage. All panels are zonal medians within the box. All data that fall on a specific grid cell on a specific year day are averaged to one value.

BGD
11, 9629–9665, 2014

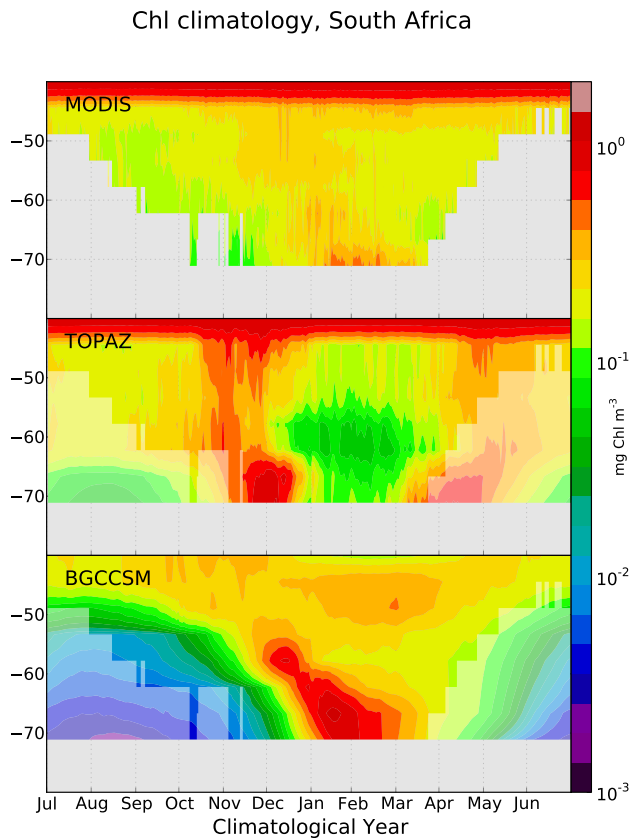

Figure 4. Hofmøller plots of satellite Chl (top panel), Chl simulated by TOPAZ (middle panel), and Chl simulated by BGCCSM (bottom panel) south of South Africa. All panels are zonal medians within the box. All data that fall on a specific grid cell on a specific year day are averaged to one value.

BGD
11, 9629–9665, 2014

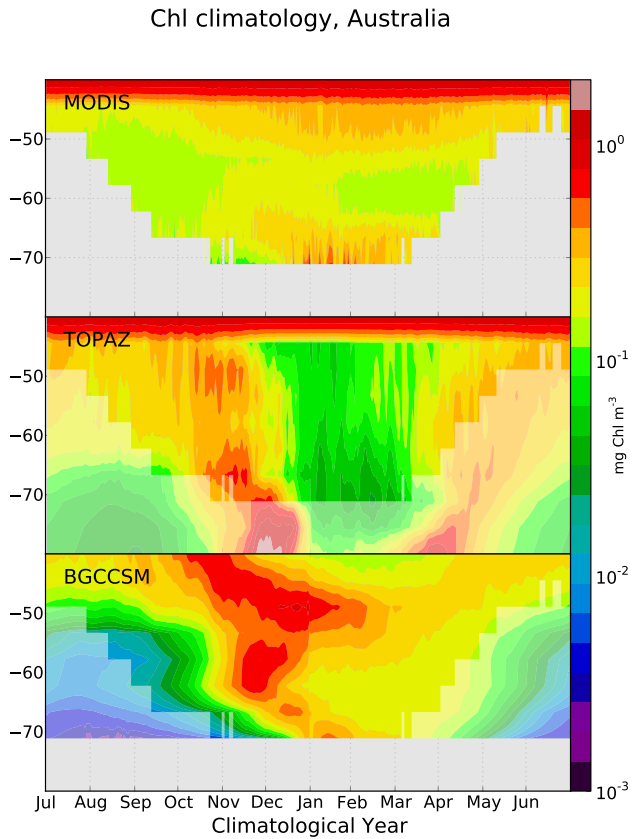

Figure 5. Hofmøller plots of satellite Chl (top panel), Chl simulated by TOPAZ (middle panel), and Chl simulated by BGCCSM (bottom panel) south of Australia. All panels are zonal medians within the box. All data that fall on a specific grid cell on a specific year day are averaged to one value.

BGD
11, 9629–9665, 2014

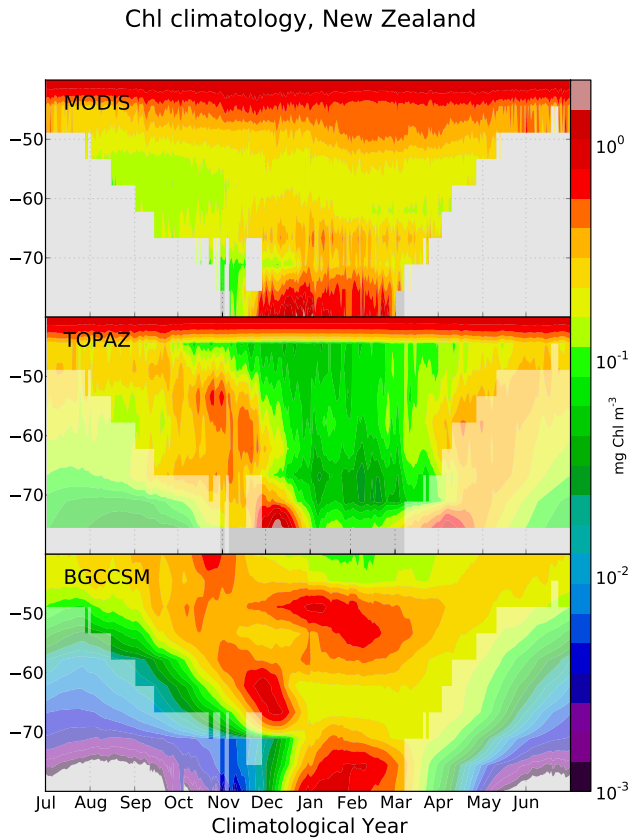

Figure 6. Hofmøller plots of satellite Chl (top panel), Chl simulated by TOPAZ (middle panel), and Chl simulated by BGCCSM (bottom panel) south of New Zealand. All panels are zonal medians within the box. All data that fall on a specific grid cell on a specific year day are averaged to one value.

BGD
11, 9629–9665, 2014

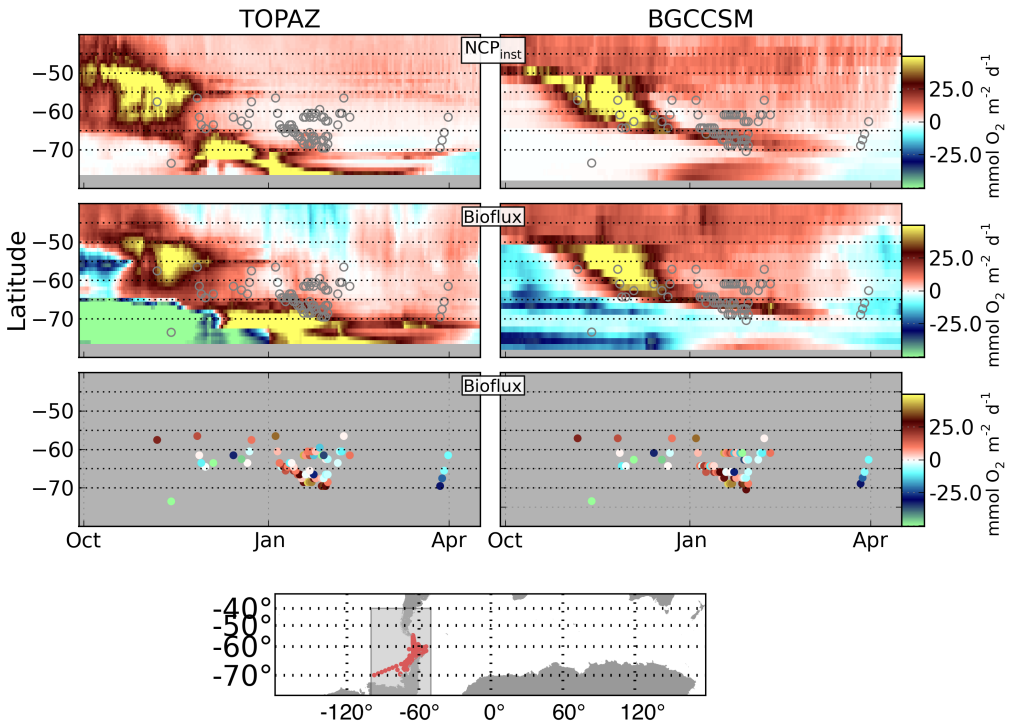

Figure 7. Hofmøller plots of model NCP (top panel), model O_2 bioflux (middle panel), and observed O2 bioflux (bottom panel) in Drake Passage (locations of observations are presented as red points in the map). All model values are zonal medians within the box. All observations that fall on a specific grid cell on a specific year day are averaged to one value.

BGD
11, 9629–9665, 2014

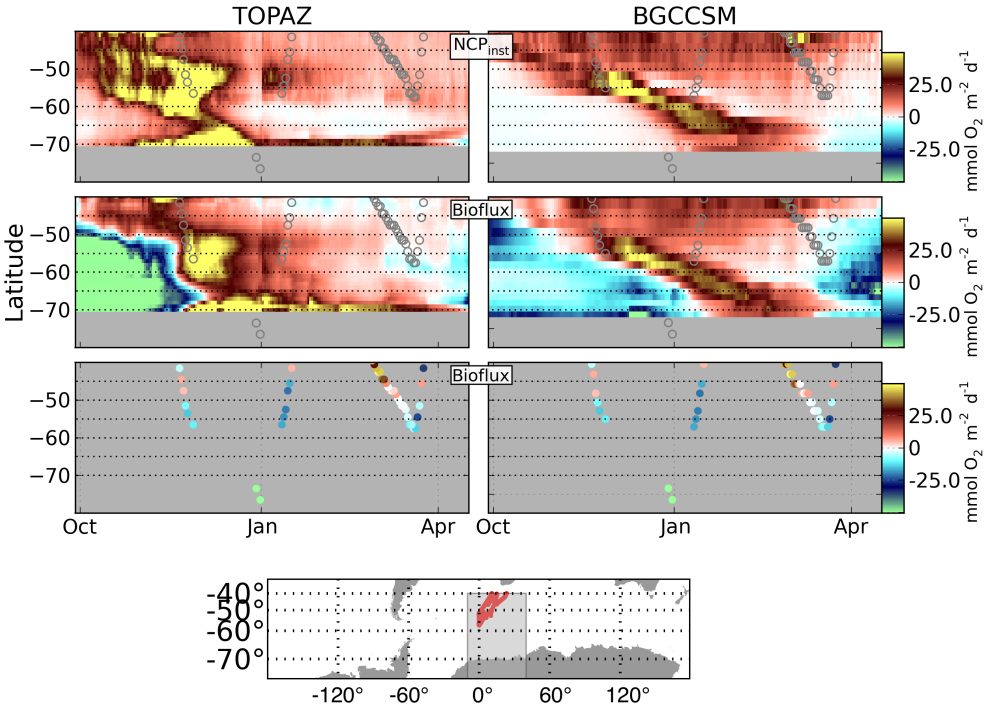

Figure 8. Hofmøller plots of model NCP (top panel), model O_2 bioflux (middle panel), and observed O_2 bioflux (bottom panel) in the Southern Ocean south of South Africa (locations of observations are presented as red points in the map). All model values are zonal medians within the box. All observations that fall on a specific grid cell on a specific year day are averaged to one value.

BGD
11, 9629–9665, 2014

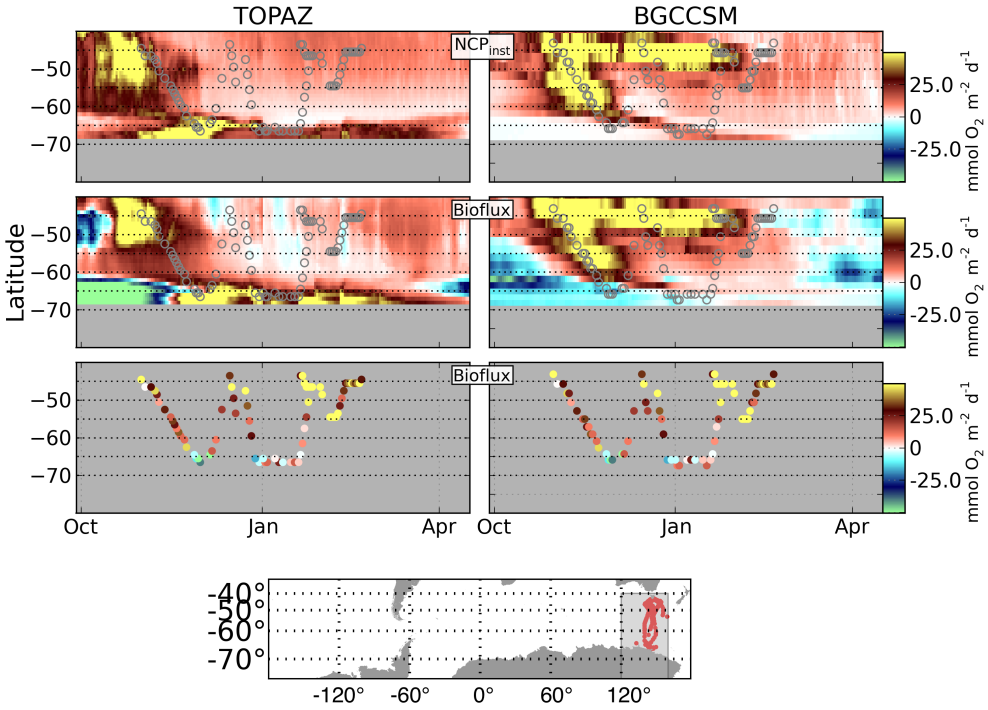

Figure 9. Hofmøller plots of model NCP (top panel), model O_2 bioflux (middle panel), and observed O_2 bioflux (bottom panel) in the Southern Ocean south of Australia (locations of observations are presented as red points in the map). All model values are zonal medians within the box. All observations that fall on a specific grid cell on a specific year day are averaged to one value.

BGD
11, 9629–9665, 2014

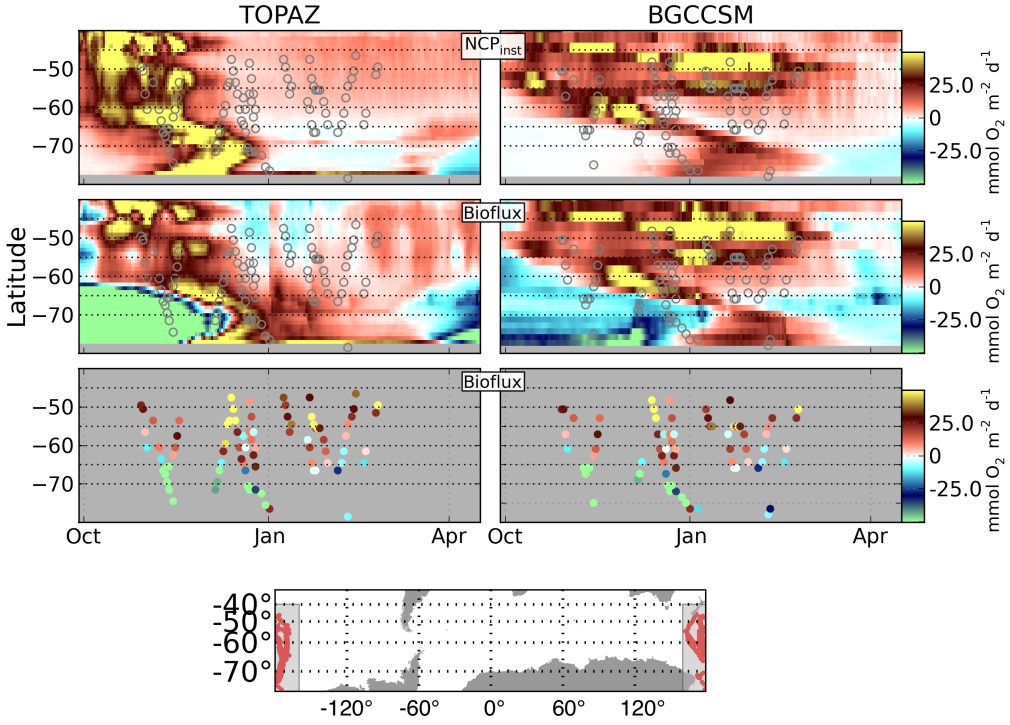

Figure 10. Hofmøller plots of model NCP (top panel), model O_2 bioflux (middle panel), and observed O_2 bioflux (bottom panel) in the Southern Ocean south of New Zealand (locations of observations are presented as red points in the map). All model values are zonal medians within the box. All observations that fall on a specific grid cell on a specific year day are averaged to one value.

BGD
11, 9629–9665, 2014

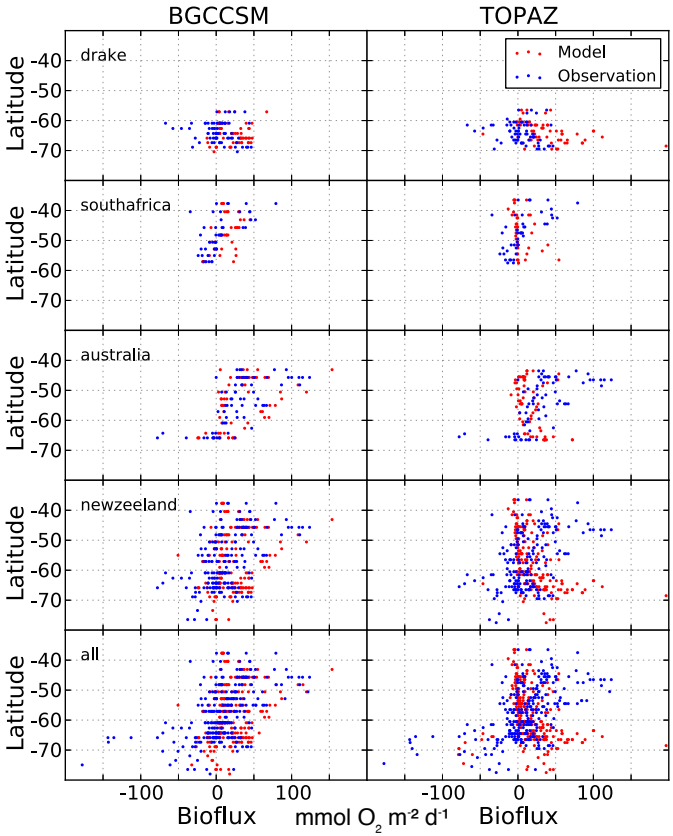

Figure 11. Scatter plots of observed (blue) and model (red) O_2 bioflux vs. latitude in four regions of the Southern Ocean. All observations that fall on a specific grid cell at a specific year day are averaged to one value. Models are subsampled at the location and year day of the observations.

BGD
11, 9629–9665, 2014

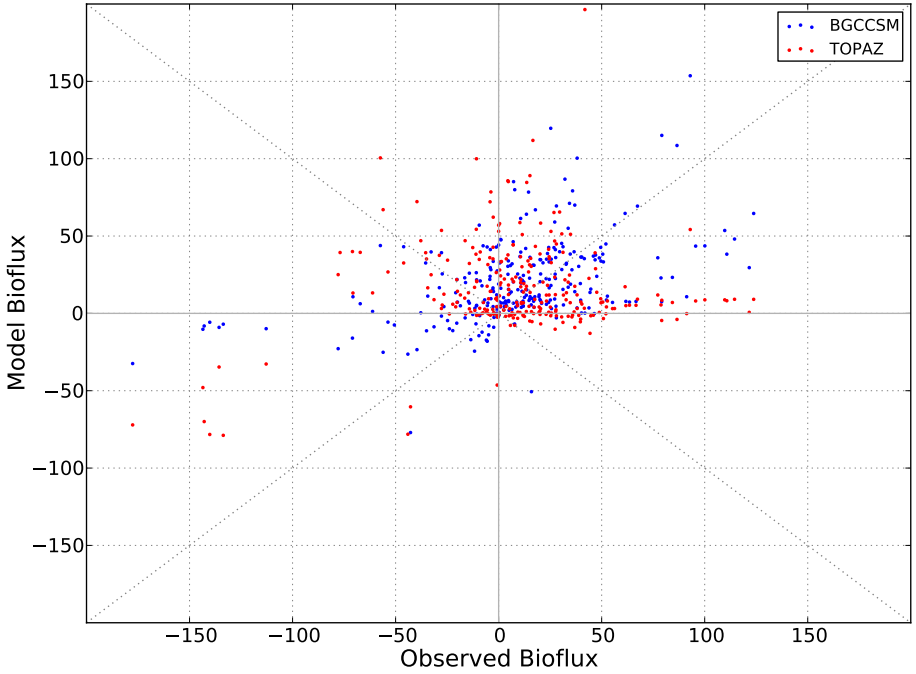

Figure 12. Scatter plots of model vs. observed O_2 bioflux for the observational sampling sites shown in Fig. 1. All observations that fall on a specific grid cell at a specific year day are averaged to one value. Models are subsampled at the location and year day of the observations.

BGD
11, 9629–9665, 2014